Fibrolite in contact aureoles of Donegal, Ireland

Derrill M. Kerrick

Department of Geosciences, The Pennsylvania State University,
University Park, Pennsylvania 16802, U.S.A.

Abstract

Fibrolite was examined in the Ardara and Fanad contact aureoles of Donegal, Ireland. Textural evidence suggests that fibrolite formed in the later stages of contact metamorphism. Garnet-biotite geothermometry and garnet-plagioclase-Al_2SiO_5-quartz geobarometry in the Ardara aureole suggest that fibrolite formed *metastably* at *P-T* conditions within the andalusite stability field. Most fibrolite is considered to have formed from the decomposition of biotite through a reaction involving acidic volatiles emanating from the adjacent intrusion. Nucleation of fibrolite, rather than the stable polymorph andalusite, may reflect the relatively high activation energy in transforming tetrahedrally coordinated Al of the biotite structure into the fivefold coordination of Al in andalusite. In contrast to fibrolite, the isograd marking the first appearance of coarse-grained sillimanite appears to correlate well with the andalusite = sillimanite equilibrium. Because fibrolitized biotite is common in metapelites of contact and regional metamorphism, interpretation of fibrolite as an equilibrium phase synonymous with coarse-grained sillimanite must be viewed with caution.

Introduction

The nature and significance of fibrolite, a common constituent of medium- to high-grade metapelites, has long been an enigma. Holdaway (1971, p. 103) concluded that "fibrolite is probably a protosillimanite which crystallizes rapidly from an irreversible mineral reaction. It may well contain excess silica and water and may have Al-Si disorder." As shown by Bell and Nord (1974) for a sample of fibrolite from Brandywine Springs, Delaware, fibrolite aggregates may indeed contain excess silica (as quartz). From their neutron-diffraction study, Finger and Prince (1972) suggested that some Al-Si disorder may exist in Brandywine Springs fibrolite. Navrotsky et al. (1973) carried out molten oxide calorimetric measurements on a sample of heat-treated Brandywine Springs fibrolite and concluded that Al-Si disorder is insignificant at temperatures below about 800°C. Experiments in the author's laboratory revealed that the *P-T* conditions of the andalusite = sillimanite equilibrium are identical regardless of whether coarse-grained sillimanite or fibrolite is used as starting material (Kerrick and Heninger, 1984). These results, coupled with the fact that coarse-grained sillimanite appears to be fully ordered (Robie and Hemingway, 1984; Peterson and McMullan, 1986), suggest that fibrolite may also be ordered. However, Salje (1986) concluded that the heat capacity of fibrolite is significantly larger than that of coarse sillimanite. Isobarically, the resultant entropy contributions yield a calculated andalusite = fibrolite equilibrium that is at a considerably higher temperature than the equilibrium involving andalusite and coarse-grained sillimanite (Salje, 1986).

Kerrick (1986) has shown that strain energy arising from dislocations is insufficient to perturb the stability relations of fibrolite compared to coarse-grained sillimanite.

A potentially significant excess energetic contribution to fibrolite arises from surface free energy. The positive surface-free-energy contribution will have the effect of destabilizing fibrolite compared to coarse sillimanite. Nitkiewicz and Kerrick (unpub. ms.) provide a detailed examination of the surface-free-energy contribution of fibrolite.

In both contact and regional metamorphic regimes, the status of fibrolite as an equilibrium phase has been questioned by several authors (Pitcher and Read, 1963; Pitcher, 1965; Chinner, 1966; Zen, 1969; Pitcher and Berger, 1972; Vernon, 1979; Speer, 1982). Because the thermal regime and history of contact aureoles are, in general, simpler than regional parageneses, this paper focuses attention on the role of fibrolite in thermal aureoles. However, some comments regarding fibrolite in regionally metamorphosed pelites are given at the end of this paper.

Analytical methods

Analyses of minerals were carried out with an automated ETEC electron-microprobe analyzer at Pennsylvania State University. Data reduction followed the Bence-Albee scheme using α factors computed according to the procedure of Albee and Ray (1970). Each mineral analysis reported in this paper represents an average of two to five individual crystals; the composition of individual crystals was obtained by averaging four to six point analyses.

Garnet, biotite, and plagioclase were analyzed for geothermometry and geobarometry (Tables 1–3). In order to utilize garnet-biotite geothermometry, the garnet analyses represent averages of *rim* compositions.

TABLE 1. Ardara aureole samples: Electron-microprobe analyses of garnet

	ARD-69-4	ARD-69-6	ARD-69-7	ARD-69-21	ARD-69-23	ARD-69-25	ARD-69-34	ARD-69-39	ARD-69-45	ARD-69-63	ARD-69-65B
SiO_2	38.26	37.94	38.26	38.09	37.86	37.89	37.66	37.80	37.27	37.17	37.66
Al_2O_3	21.33	21.06	21.07	20.79	21.37	21.74	20.48	21.42	21.45	24.56	21.25
TiO_2	0.08	0.17	0.04	0.18	0.05	0.07	0.05	0.05	0.02	0.12	0.17
MgO	2.03	2.20	2.29	2.27	1.78	2.26	1.92	3.02	1.98	1.22	1.52
FeO	32.83	31.45	31.23	32.15	34.95	28.49	34.84	36.35	31.89	26.20	27.25
MnO	5.66	6.35	6.01	5.00	3.78	7.04	3.17	0.99	6.45	5.76	5.15
CaO	1.48	1.64	1.98	1.81	1.62	2.93	1.37	1.33	1.49	5.68	6.93
Na_2O	0.00	0.01	0.05	0.01	0.00	0.06	0.00	0.02	0.00	0.00	0.00
K_2O	0.03	0.05	0.05	0.04	0.03	0.02	0.03	0.01	0.01	0.03	0.05
Σ	101.70	100.85	100.98	100.34	101.44	100.50	99.52	100.99	100.56	100.74	99.98
					Formula basis: 12 oxygens						
Si	3.035	3.033	3.047	3.053	3.020	3.018	3.058	3.009	2.998	2.924	3.012
Al	1.996	1.985	1.979	1.965	2.010	2.040	1.960	2.011	2.034	2.268	2.004
Ti	0.005	0.010	0.002	0.011	0.003	0.004	0.003	0.003	0.001	0.007	0.010
Mg	0.240	0.263	0.272	0.271	0.211	0.267	0.232	0.358	0.237	0.143	0.181
Fe	2.178	2.102	2.080	2.155	2.332	1.899	2.366	2.420	2.145	1.725	1.822
Mn	0.380	0.430	0.405	0.339	0.255	0.475	0.218	0.067	0.439	0.385	0.349
Ca	0.126	0.140	0.169	0.155	0.138	0.250	0.119	0.113	0.128	0.481	0.594
Na	0.001	0.002	0.008	0.001	0.000	0.009	0.001	0.003	0.000	0.000	0.000
K	0.004	0.005	0.006	0.004	0.003	0.002	0.003	0.001	0.001	0.003	0.005
Σ	7.964	7.968	7.968	7.956	7.973	7.964	7.961	7.985	7.985	7.936	7.978
X_{Al}	0.745	0.716	0.711	0.738	0.794	0.656	0.806	0.818	0.727	0.634	0.618
X_{Py}	0.082	0.089	0.093	0.093	0.072	0.093	0.079	0.121	0.080	0.053	0.061
X_{Gr}	0.043	0.048	0.058	0.053	0.047	0.087	0.041	0.038	0.044	0.173	0.201
X_{Sp}	0.130	0.146	0.139	0.116	0.087	0.164	0.074	0.022	0.149	0.140	0.119

	ARD-85-1A	ARD-85-1B	ARD-85-1C	ARD-85-2A	ARD-85-15	ARD-85-16	ARD-85-17	ARD-85-26A	ARD-85-31A	ARD-85-32A	ARD-85-33
SiO_2	37.81	37.91	37.18	38.13	37.10	37.58	37.91	38.12	37.45	37.69	37.56
Al_2O_3	21.38	20.69	21.01	20.63	21.17	21.38	21.48	20.80	21.27	21.17	20.58
MgO	3.59	3.34	3.22	3.24	2.51	2.52	2.63	2.57	2.32	2.16	2.16
FeO	36.37	35.64	36.10	36.24	29.26	31.61	31.47	26.72	30.38	34.03	30.38
MnO	1.05	0.82	1.31	1.13	8.41	6.35	5.80	4.77	6.83	4.53	8.70
CaO	1.05	1.97	1.38	1.44	2.12	1.80	2.03	7.36	2.90	1.73	1.20
Σ	101.25	100.37	100.20	100.81	100.57	101.24	101.32	100.34	100.34	101.30	100.58
					Formula basis: 12 oxygens						
Si	3.000	3.033	2.992	3.043	2.983	2.997	3.010	3.027	3.008	3.011	3.029
Al	2.001	1.951	1.994	1.941	2.007	2.011	2.011	1.947	2.014	1.995	1.957
Mg	0.425	0.398	0.386	0.385	0.300	0.300	0.311	0.304	0.278	0.257	0.259
Fe	2.414	2.385	2.430	2.418	1.968	2.108	2.089	1.774	2.041	2.274	2.049
Mn	0.071	0.056	0.089	0.077	0.573	0.429	0.390	0.321	0.465	0.306	0.594
Ca	0.089	0.169	0.119	0.123	0.183	0.154	0.173	0.627	0.180	0.148	0.104
Σ	8.000	7.992	8.011	7.987	8.014	7.998	7.985	8.000	7.985	7.991	7.992
X_{Al}	0.805	0.793	0.804	0.805	0.651	0.705	0.705	0.586	0.689	0.762	0.682
X_{Py}	0.142	0.132	0.128	0.128	0.099	0.100	0.105	0.101	0.094	0.086	0.086
X_{Gr}	0.030	0.056	0.039	0.041	0.061	0.051	0.058	0.207	0.061	0.050	0.034
X_{Sp}	0.024	0.018	0.030	0.026	0.189	0.143	0.132	0.106	0.157	0.103	0.198

The Al_2SiO_5 phases were analyzed (Table 4) in order to evaluate the role of minor-element solid solution, with particular emphasis on the effect of solid solution on the andalusite = fibrolite equilibrium. Microprobe analyses of fibrolite were obtained in selected areas that contained minimal contaminant phases. Quartz was found to be the major contaminant of fibrolite. Areas containing quartz were readily identified by the characteristic blue cathodoluminescence of this phase and/or by SiO_2 contents in excess of the Al_2SiO_5 stoichiometry. The amount of quartz included within the fibrolites examined in this study was computed assuming a linear relation between the SiO_2 content of stoichiometric Al_2SiO_5 ($SiO_2 = 37.09$ wt%) and quartz ($SiO_2 = 100$ wt%). In essence, the SiO_2 in excess of 37.09 wt% was assigned to quartz. From the SiO_2 values of fibrolite in Table 4, the quartz contamination was a maximum of 1.4 wt% (sample ARD-85-16); fibrolites analyzed in most other samples contain less than 1 wt% quartz.

DONEGAL AUREOLES

General geologic setting

The geology of the Donegal region of northern Ireland has been thoroughly reviewed by Pitcher and Berger (1972), and the chronology of the sedimentary, tectonic, and igneous history has been summarized by Powell and Phillips (1985). In brief, the country rocks of Donegal consist of Dalradian metasedimentary and meta-igneous rocks that range in age from late Precambrian to Middle Cambrian. This group of rocks subsequently underwent major deformation (the Caledonian orogeny) during Late Cambrian to Late Ordovician time. Intrusion of the Donegal granites is considered to have occurred at about 390–405 Ma (Halliday et al., 1980).

TABLE 2. Ardara aureole samples: Electron-microprobe analyses of biotite

	ARD-69-4	ARD-69-6	ARD-69-7	ARD-69-21	ARD-69-23	ARD-69-25	ARD-69-34	ARD-69-39	ARD-69-45	ARD-69-63	ARD-69-65B
SiO_2	35.91	37.31	36.00	35.36	34.79	36.21	35.65	35.23	35.17	31.07	34.84
Al_2O_3	20.32	21.07	19.80	18.55	20.18	19.79	18.98	20.13	19.44	21.50	19.96
TiO_2	2.00	1.39	1.84	2.37	1.98	1.91	2.47	2.24	2.37	0.89	1.42
MgO	8.07	9.16	10.11	7.65	7.69	9.25	7.85	8.21	7.78	12.06	10.72
FeO	21.32	18.11	17.98	21.74	22.27	18.76	21.63	20.32	20.74	20.53	18.32
MnO	0.14	0.07	0.16	0.16	0.04	0.14	0.12	0.08	0.15	0.11	0.07
CaO	0.00	0.00	0.01	0.00	0.00	0.02	0.00	0.00	0.01	0.03	0.00
Na_2O	0.18	0.14	0.20	0.09	0.14	0.22	0.21	0.35	0.11	0.04	0.23
K_2O	7.19	7.36	8.06	7.83	7.36	8.31	7.35	7.97	8.34	3.18	6.35
Σ	95.13	94.61	94.16	93.76	94.45	94.61	94.26	94.53	94.11	89.41	91.91
						Formula basis: 22 oxygens					
Si	5.429	5.559	5.448	5.482	5.345	5.476	5.470	5.377	5.419	4.907	5.368
^{IV}Al	2.571	2.441	2.552	2.518	2.655	2.524	2.530	2.623	2.581	3.093	2.632
^{VI}Al	1.051	1.260	0.980	0.874	0.999	1.008	0.905	0.999	0.950	0.937	0.995
Ti	0.228	0.156	0.210	0.276	0.229	0.218	0.285	0.257	0.275	0.104	0.165
Mg	1.819	2.034	2.281	1.768	1.761	2.073	1.797	1.868	1.787	2.862	2.464
Fe	2.696	2.257	2.276	2.819	2.861	2.386	2.776	2.594	2.673	2.730	2.363
Mn	0.018	0.009	0.021	0.022	0.006	0.018	0.015	0.010	0.019	0.015	0.009
Σ	5.812	5.715	5.767	5.758	5.857	5.703	5.777	5.728	5.704	6.648	5.995
Ca	0.000	0.000	0.002	0.000	0.000	0.003	0.000	0.000	0.002	0.006	0.000
Na	0.054	0.040	0.059	0.027	0.041	0.063	0.063	0.104	0.032	0.013	0.070
K	1.386	1.399	1.556	1.549	1.443	1.607	1.439	1.552	1.638	0.628	1.248
Σ	1.441	1.439	1.617	1.576	1.484	1.673	1.502	1.655	1.673	0.647	1.317
X_{Ph}	0.314	0.356	0.397	0.308	0.301	0.364	0.312	0.327	0.314	0.428	0.411
X_{Ann}	0.465	0.395	0.396	0.491	0.489	0.420	0.482	0.454	0.470	0.411	0.395

	ARD-85-1A	ARD-85-1B	ARD-85-1C	ARD-85-2A	ARD-85-15	ARD-85-16	ARD-85-17	ARD-85-26A	ARD-85-31A	ARD-85-32A	ARD-85-33
SiO_2	35.54	35.59	35.51	34.97	36.05	35.21	36.51	35.56	36.08	35.32	34.79
Al_2O_3	19.95	19.37	19.89	20.05	19.51	20.11	20.03	19.49	19.98	19.47	19.74
TiO_2	2.20	2.50	2.12	2.58	1.67	1.92	1.57	1.40	1.59	1.90	2.49
MgO	9.10	10.27	8.60	8.10	11.10	10.39	10.85	14.14	10.75	8.51	7.93
FeO	20.07	18.35	21.18	20.42	18.01	18.02	17.37	14.50	18.07	20.97	20.98
MnO	0.03	0.04	0.00	0.07	0.15	0.08	0.07	0.15	0.13	0.01	0.13
CaO	0.00	0.00	0.00	0.00	0.02	0.00	0.00	0.00	0.00	0.00	0.00
Na_2O	0.34	0.26	0.23	0.21	0.18	0.30	0.32	0.20	0.21	0.20	0.20
K_2O	7.88	7.86	7.93	8.99	7.56	7.95	7.95	6.96	7.72	7.70	6.94
Σ	95.11	94.24	95.46	95.39	94.25	93.98	94.67	92.40	94.53	94.04	93.38
						Formula basis: 22 oxygens					
Si	5.377	5.394	5.381	5.326	5.437	5.347	5.466	5.370	5.427	5.424	5.372
^{IV}Al	2.623	2.606	2.619	2.674	2.563	2.653	2.534	2.630	2.573	2.576	2.628
^{IV}Al	0.936	0.856	0.934	0.928	0.907	0.948	1.002	0.841	0.970	0.949	0.965
Ti	0.250	0.285	0.242	0.296	0.190	0.220	0.177	0.159	0.180	0.219	0.289
Mg	2.053	2.320	1.942	1.839	2.495	2.352	2.421	3.184	2.411	1.947	1.825
Fe	2.539	2.326	2.684	2.601	2.272	2.289	2.175	1.832	2.274	2.693	2.709
Mn	0.004	0.006	0.000	0.009	0.019	0.010	0.009	0.020	0.016	0.002	0.041
Σ	5.782	5.793	5.801	5.672	5.883	5.819	5.784	6.036	5.850	5.811	5.829
Ca	0.000	0.000	0.000	0.000	0.003	0.000	0.000	0.000	0.000	0.000	0.000
Na	0.100	0.077	0.067	0.063	0.052	0.088	0.094	0.059	0.062	0.060	0.060
K	1.521	1.519	1.533	1.747	1.454	1.540	1.518	1.340	1.482	1.508	1.367
Σ	1.622	1.596	1.600	1.810	1.509	1.628	1.612	1.398	1.543	1.568	1.427
X_{Ph}	0.355	0.401	0.335	0.325	0.425	0.405	0.419	0.529	0.413	0.335	0.315
X_{Ann}	0.439	0.402	0.463	0.459	0.387	0.394	0.377	0.304	0.390	0.464	0.468

Ardara aureole

The Ardara pluton (Fig. 1) represents a forcibly emplaced, diapiric intrusion (Holder, 1979; Sanderson and Meneilly, 1981). This pluton consists of an outer carapace of quartz monzodiorite (230–900 m thick) enclosing a granodiorite core (Akaad, 1956a). Pitcher and Berger (1972, p. 182) considered that these two intrusive phases were closely spaced in time. The highly foliated structure of the outer quartz monzodiorite, coupled with strong deformation of the country rocks, provides clear evidence for the diapiric character of the Ardara pluton.

The northern Ardara aureole, which is the focus of the present investigation, consists of a pelitic horizon (locally referred to as the Clooney Pelitic Group) and an adjacent limestone unit (the Portnoo Limestone). Pitcher and Berger (1972) correlated these units with the respective Upper Falcarragh Pelites and the Falcarragh Limestone, which are members of the Creeslough Succession that forms the country rock for most of the Donegal intrusions (see Pitcher and Berger, 1972, Fig. 1-1). In detail, the pelitic horizon of the northern Ardara aureole consists of interlayered aluminous pelites and semipelites. Lenses and

TABLE 3. Ardara aureole samples: Electron-microprobe analyses of zoned plagioclase

	ARD-85-1B		ARD-85-1C		ARD-85-10	
	Core	Rim	Core	Rim	Core	Rim
SiO_2	57.94	61.44	57.92	67.72	56.77	62.12
Al_2O_3	26.15	23.90	26.42	24.12	27.39	23.47
FeO	—	—	0.05	—	N.D.	N.D.
CaO	8.80	6.08	9.90	6.74	9.05	4.91
Na_2O	6.13	7.44	5.75	6.97	6.27	8.78
K_2O	0.02	0.03	N.D.	N.D.	—	—
	99.04	98.89	100.11	100.55	99.49	99.29
Formula basis: 8 oxygens						
Si	2.611	2.748	2.589	2.755	2.555	2.768
Al	1.389	1.260	1.396	1.248	1.452	1.231
Fe	—	—	0.001	0.001	—	—
Ca	0.425	0.291	0.474	0.316	0.436	0.234
Na	0.536	0.645	0.497	0.593	0.546	0.758
K	0.001	0.002	N.D.	N.D.	—	—
X_{An}	0.442	0.310	0.488	0.348	0.444	0.236
X_{Ab}	0.557	0.688	0.512	0.652	0.556	0.764
X_{Or}	0.001	0.002	N.D.	N.D.	—	—

pods of metadolerite are common in a zone extending about 200 m from the plutonic contact (Akaad, 1956b).

Figure 1 shows the metamorphic zones in the northern Ardara aureole. Accordingly, the aureole is subdivided into an outer zone characterized by andalusite + kyanite, an intermediate zone with andalusite, and an inner zone containing coarse, prismatic sillimanite (*hereafter referred to as sillimanite*). The extent of the andalusite + kyanite zone was not confirmed in this study, as kyanite was identified in only one sample (ARD-85-30). If fibrolite is excluded, the sillimanite isograd is abrupt and well defined. From electron-microprobe analyses of minor-element contents of andalusite and sillimanite, Ker-

rick and Speer (1987) have concluded that the andalusite → sillimanite isograd reaction represents a close analogue to the univariant andalusite = sillimanite equilibrium involving pure phases. Pitcher and Read (1963) concluded that the metamorphic zone characterized by fibrolite is relatively narrow; however, fibrolite is actually abundant in andalusite-bearing rocks, extending to a distance of about 400 m from the intrusive contact (Fig. 1B).

Within the andalusite-bearing rocks, garnet occurs as small, rounded porphyroblasts. In contrast, within the sillimanite zone, garnet occurs as larger crystals that are, in several specimens, irregular in shape. The garnet texture, as well as the overall texture of the rock, suggests that the transformation from the andalusite to sillimanite zones was accompanied by a wholesale textural reconstitution.

In several samples, andalusite porphyroblasts have pink cores surrounded by colorless rims. This zoning is quite common in porphyroblastic andalusite (Okrusch and Evans, 1970). Electron-microprobe analysis (Kerrick and Speer, 1987) shows that the cores contain higher concentrations of Fe compared to the rims; however, there appear to be no significant differences in the concentrations of other minor elements between cores and rims.

Replacement reaction has been significant in many samples from the northern Ardara aureole. Andalusite has undergone varying degrees of replacement by muscovite. In many samples, replacement is complete, yielding coarse-grained ovoids of interlocking muscovites surrounded by coarse-grained biotite. In several specimens, well-developed muscovite porphyroblasts have replaced biotite (Fig. 2A). The temporal relationship of these porphyroblasts to the muscovite that has replaced andalusite porphyroblasts is unknown.

TABLE 4. Ardara aureole samples: Electron-microprobe analyses of aluminum silicates

	ARD-85-1A F	ARD-85-2A F	ARD-85-3E F	ARD-85-5A F	ARD-85-10 F	ARD-85-15 A	ARD-85-16		ARD-85-17		ARD-85-32A A	ARD-69-34 F	ARD-69-65B A
							A	F	A	F			
SiO_2	36.95	37.52	37.65	37.54	37.51	36.27	36.66	37.96	36.94	37.80	36.88	37.05	37.09
Al_2O_3	61.66	62.59	61.63	61.11	62.05	62.73	62.53	60.72	62.52	61.38	61.81	61.83	62.24
TiO_2	0.01	n.d.	n.d.	0.07	0.01	0.05	0.05	0.00	0.00	0.00	0.03	0.06	0.02
Fe_2O_3	0.27	0.38	0.15	0.18	0.18	0.26	0.26	0.43	0.17	0.62	0.29	0.19	0.19
Cr_2O_3	0.15	0.02	0.01	0.02	0.13	0.04	0.03	0.01	0.00	0.00	0.03	0.12	0.13
MnO	0.05	0.01	0.02	0.03	0.02	0.01	0.01	0.03	0.00	0.00	0.01	0.01	0.02
MgO	0.00	0.07	0.02	0.01	0.00	n.d.	0.02	0.22	0.07	0.27	0.05	0.02	0.04
Σ	99.09	100.59	99.48	98.96	99.90	99.36	99.56	99.37	99.70	100.07	99.10	99.28	99.73
Formula basis: 5 oxygens													
Si	1.007	1.007	1.020	1.023	1.013	0.986	0.994	1.031	1.000	1.020	1.005	1.007	1.004
Al	1.981	1.981	1.969	1.963	1.976	2.011	2.000	1.944	1.995	1.953	1.985	1.982	1.986
Ti	0.000	n.d.	n.d.	0.001	0.000	0.001	0.001	0.000	0.000	0.000	0.001	0.001	0.001
Fe	0.006	0.008	0.003	0.004	0.004	0.005	0.005	0.009	0.003	0.013	0.006	0.004	0.004
Cr	0.003	0.000	0.000	0.000	0.003	0.001	0.001	0.000	0.000	0.000	0.001	0.003	0.003
Mn	0.001	0.000	0.000	0.001	0.000	0.000	0.000	0.001	0.000	0.000	0.000	0.000	0.001
Mg	0.000	0.003	0.001	0.001	0.000	n.d.	0.001	0.009	0.003	0.011	0.002	0.001	0.002
Σ	2.998	2.999	2.994	2.992	2.996	3.005	3.002	2.993	3.001	2.997	2.999	2.998	2.999
X_{viM}	0.010	0.011	0.004	0.007	0.007	0.007	0.008	0.019	0.006	0.023	0.010	0.009	0.009
X_{viAl}	0.990	0.989	0.996	0.993	0.993	0.993	0.992	0.981	0.994	0.977	0.990	0.991	0.991
							$K = 0.989$		$K = 0.983$				

Note: A = andalusite, S = sillimanite, F = fibrolite. $K = X^{Fib}_{viAl^{v}AlSiO_5} / X^{And}_{viAl^{v}AlSiO_5}$.
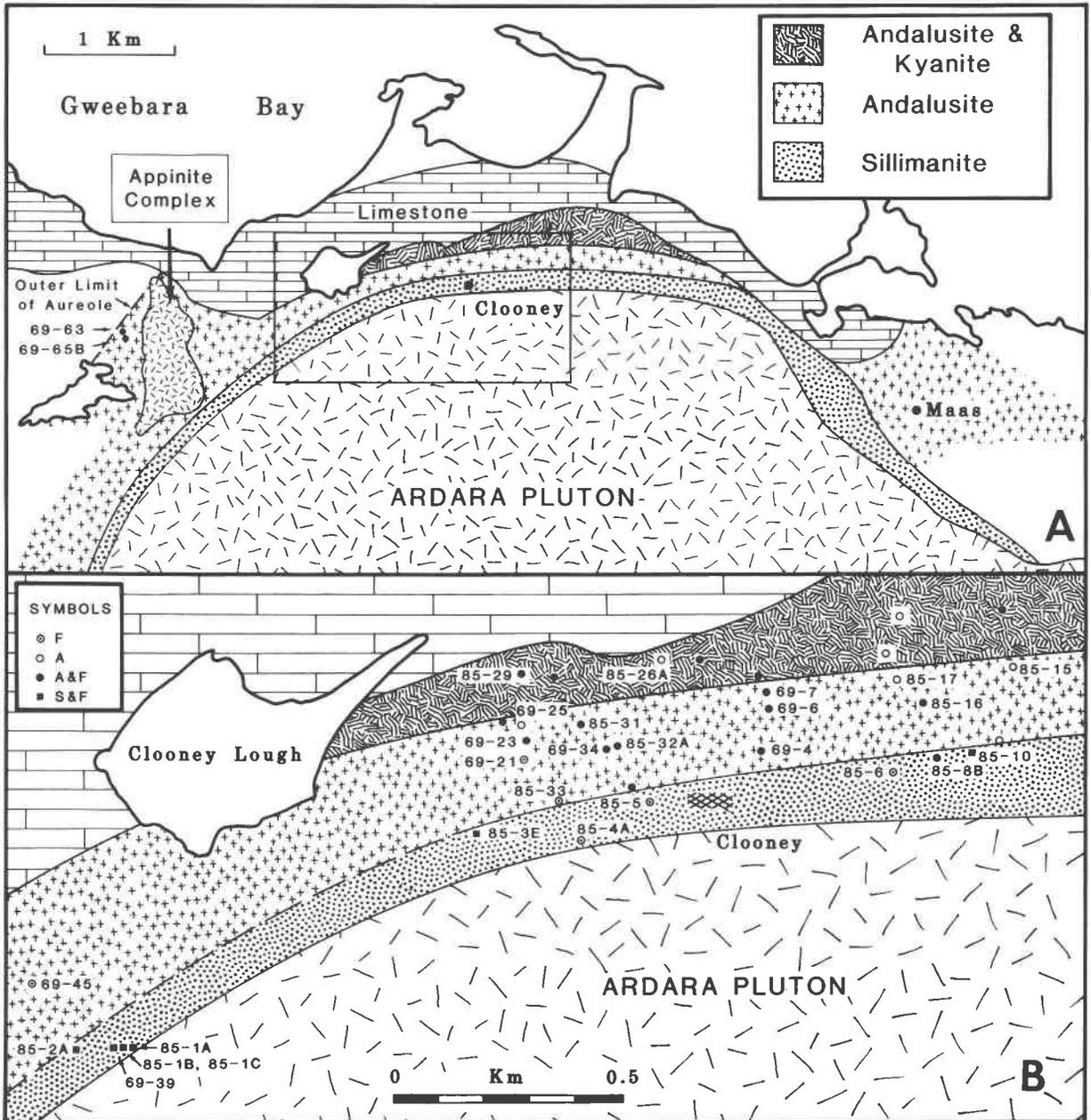
Fig. 1.   (A) Geology of the northern portion of the Ardara pluton and surrounding country rock (from Pitcher and Berger, 1972, Fig. 14-6). The rectangular area encompassing Clooney is the area covered by Fig. 1B. The locations of two samples (ARD-69-63 and ARD-69-65B) are shown near the outer limit of the aureole. (B) Sample-locality map of the northern Ardara aureole, showing aluminum silicate assemblages. The ARD prefix (used to designate these samples in the text and tables) is omitted for clarity.

Biotite has undergone two major replacement reactions. First, chloritization of biotite occurs in some samples. Second, and of paramount importance to this investigation, biotite in many samples throughout the aureole has undergone varying degrees of replacement by fibrolite. As illustrated by Figures 2B and 2C, the fibrolitization of biotite is clearly a *replacement* reaction (cf. Chinner, 1961). Fibrolite also occurs in stringers that are parallel to the foliation. In many samples it is obvious

that these stringers replace biotite, but in others there is no clear evidence of a biotite precursor. Within the sillimanite zone, fibrolitization of biotite is well advanced in many specimens examined. However, in this zone, fibrolite also occurs as a product of garnet decomposition (Fig. 2E) and as concentrations at grain boundaries (Fig. 2F).

In a few samples, fibrolite occurs within muscovite crystals. The relative timing of growth of these phases is

uncertain, although the presence of well-developed fibrolite needles suggests that the muscovite did not replace fibrolite. Pitcher and Read (1963) concluded that inclusions of fibrolite within muscovite suggest contemporaneous growth of these phases.

In most samples, fibrolite is spatially unassociated with andalusite or sillimanite (Fig. 2D). In essence, fibrolite did not nucleate on or within a pre-existing Al_2SiO_5 mineral. Furthermore, within the andalusite and andalusite-kyanite zones, fibrolitized biotite occurs in several samples that lack andalusite and that show no textural evidence (i.e., muscovite-rich patches) suggestive of andalusite porphyroblasts that have been completely replaced.

Fanad aureole

The Fanad granodiorite is the northernmost of the Donegal granites. This pluton consists of an outer zone of migmatitic quartz monzonite enclosing a xenolith-rich granodiorite core. As with the Ardara pluton, the foliation becomes more prominent as the external contact is approached.

The aureole of the Fanad granodiorite was studied in a pelitic horizon on the eastern shore of Mulroy Bay, north of the hamlet of Glinsk (Fig. 3). This area was the subject of several previous investigations (Pitcher and Read, 1963; Naggar and Atherton, 1970; Edmunds and Atherton, 1971). The pelitic horizon in this region is part of the Sessiagh-Clonmass Formation, which is part of the Dalradian Creeslough Succession. Pitcher and Berger (1972) consider that the Sessiagh-Clonmass Formation is older than the upper Falcarragh pelites of the northern Ardara aureole. Outside of the aureole, the pelite is a garnetiferous schist. Accordingly, the Fanad aureole formed from a protolith that had been metamorphosed to the greenschist facies by an earlier regional metamorphism.

The salient features of prograde metamorphism in the Glinsk area were summarized by Naggar and Atherton (1970), Edmunds and Atherton (1971), and Pitcher and Berger (1972). The outer limit of the aureole is marked by the first appearance of biotite within the precursor quartz-chlorite-muscovite-garnet schist. Prograde metamorphism is delineated by a series of well-defined isograds (Fig. 3). Edmunds and Atherton (1971) traced the prograde chemical evolution of garnet within the contact aureole. Through microprobe analysis they were able to distinguish garnet cores, correlative with unresorbed regionally metamorphosed garnet, and rim compositions representing garnet grown during contact metamorphism.

Isograd number 8 in Figure 3 was designated by Edmunds (1969) as the disappearance of muscovite coupled with the appearance of fibrolite. However, samples collected by the author result in a different location for the fibrolite-in isograd (isograd number 6 in Fig. 3). Furthermore, in contrast to Edmunds' (1969) study, this study shows that muscovite persists into the sillimanite zone. Although some muscovite in the higher-grade rocks appears to be secondary, muscovite within biotite-rich knots (which were probably garnet porphyroblasts in the protolith) could well be primary.

As in the Ardara aureole, fibrolite is dominantly intergrown with biotite. This biotite-fibrolite association occurs from the fibrolite isograd through the sillimanite zone. As shown in Figures 2G and 2H, textures demonstrate that fibrolite formed from the breakdown of biotite. With rare exception, fibrolite shows no evidence of nucleating on or within andalusite or sillimanite.

The sillimanite zone is characterized by the coexistence of sillimanite, andalusite, and fibrolite. Sillimanite is intergrown with, and has replaced, andalusite.

ANALYSIS OF FIBROLITE FORMATION

P-T conditions

To assess the physicochemical conditions of contact metamorphism, and to address the P-T conditions of fibrolite formation, thermobarometry was determined using the garnet-biotite Mg-Fe exchange equilibrium (Ferry and Spear, 1978) and the garnet-plagioclase-Al_2SiO_5-quartz geobarometer (Ghent, 1976; Ghent et al., 1979).

The garnet-biotite thermometry is summarized in Table 5. Uncertainties given in this table for the temperatures obtained by the Ferry-Spear equation were derived using a standard error for the equilibrium constant computed as in Hodges and Spear (1982, p. 1126). In so doing, it was assumed that each of the mole fractions used in computing the equilibrium constant had standard errors of 3% *relative*. Ferry and Spear (1978) recommend that their garnet-biotite geothermometer may be used with $(Ca + Mn)/(Ca + Mn + Fe + Mg) \leq 0.2$ in garnet and $(^{VI}Al + Ti)/(^{VI}Al + Ti + Fe + Mg) \leq 0.15$ in biotite. This requirement is fulfilled for most of the analyzed garnets (Table 1), although most biotites analyzed from the Ardara samples (Table 2) have $(^{VI}Al + Ti)/(^{VI}Al + Ti + Fe + Mg) \simeq 0.20$. Hodges and Spear (1982) reformulated the Ferry and Spear (1978) geothermometer by accounting for nonideal mixing in garnet. The Hodges and Spear (1982) activity coefficients for the pyrope and almandine components were derived from a symmetric, four-component regular solution model using the Ca-Mg binary interaction parameter (W_{Ca-Mg}) of Newton et al. (1977) and assuming the other binary interaction parameters to be zero. As shown in Table 5, the temperatures calculated from the Ferry and Spear (1978) versus Hodges and Spear (1982) formulations differ between 2 and 8 deg for most samples. However, the temperature differences are 20–25 deg for three samples (69-63, 69-65B, and 85-26A) that contain significant Ca contents. In comparison with most other samples, biotites in these three samples have lower microprobe totals, in part attributable to lower K_2O contents. Although not obvious petrographically, these biotites may be altered. Therefore, the temperatures determined by garnet-biotite thermometry for these three samples *may* not represent those of the thermal maxima.

Using the garnet-plagioclase-Al_2SiO_5-quartz geobarometer in sillimanite-zone rocks of the Ardara aureole,
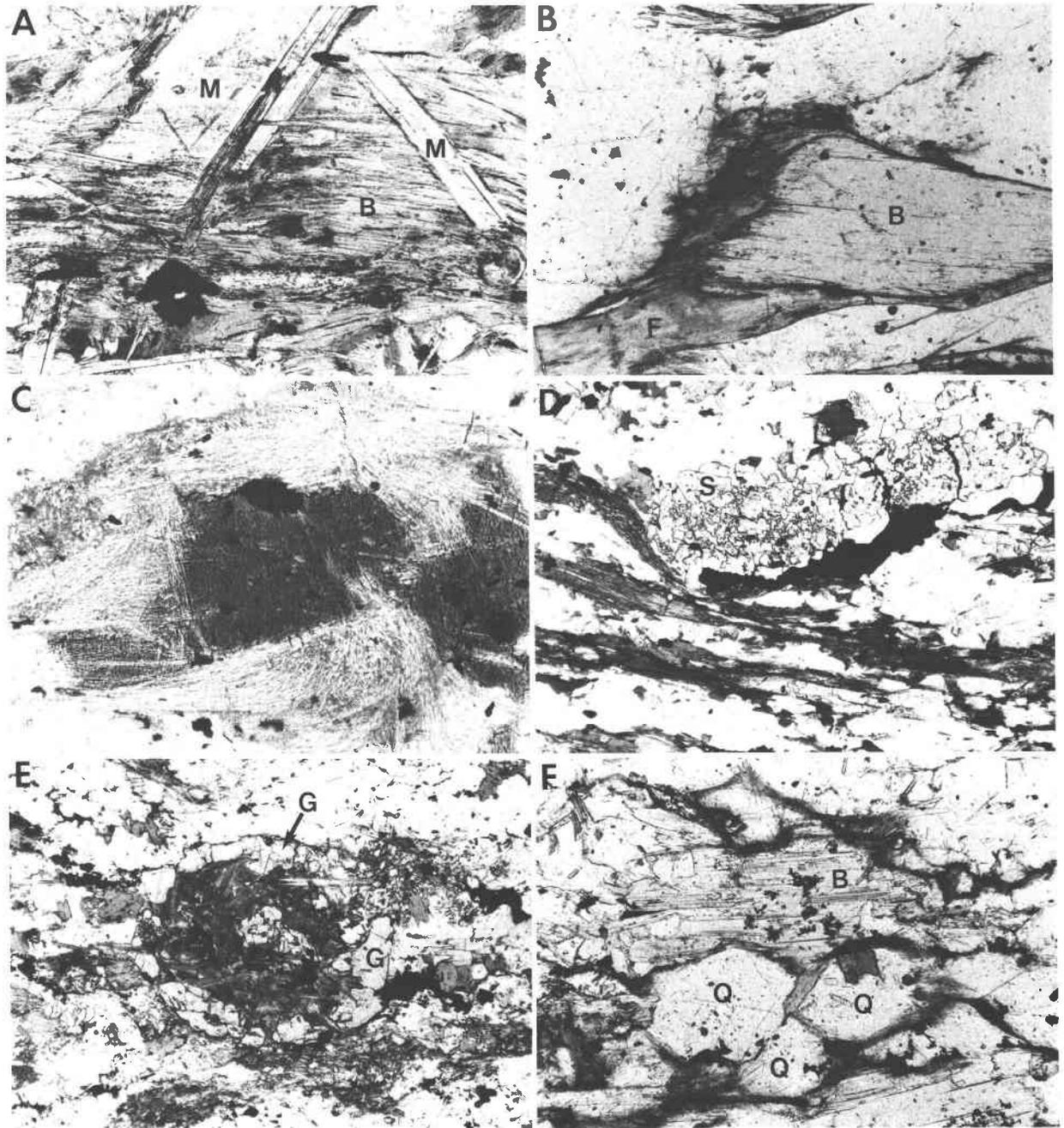
Fig. 2. Photomicrographs of samples from the Ardara (ARD prefix) and Fanad (GL prefix) aureoles. (A) Late muscovite (M) cross-cutting biotite (B) (sample ARD-85-31). The foliation of the biotite is preserved as inclusion trails in the muscovite. Width of photo corresponds to 1.3 mm. (B) Biotite (B) fringed by fibrolite (F) (sample ARD-85-10). Width of photo corresponds to 2.6 mm. (C) Biotite with surrounding fibrolite (sample ARD-85-3E). Width of photo corresponds to 0.65 mm. (D) Prismatic sillimanite (S) with adjacent layers of fibrolitized biotite (dark layers in lower portion of photo) (sample ARD-85-10). Width of photo corresponds to 2.6 mm. (E) Garnet (G) replaced by fibrolite + pyrrhotite (sample ARD-85-1C). Width of photo corresponds to 2.6 mm. (F) Fibrolite at grain boundaries (sample ARD-85-3E). Selected grains of biotite (B) and quartz (Q) are noted. Width of photo corresponds to 1.3 mm.

the rim compositions of zoned plagioclase yield pressures (4–5 kbar) well beyond the stability limit of andalusite; however, core compositions yield pressures in the range of 2–3 kbar. Electron-microprobe traverses show that the

plagioclase consists of a homogeneous, calcic core surrounded by a sodic rim (see Table 3) and that there is a sharp discontinuity between the core and rim. The sodic rims have compositions similar to the plagioclase in
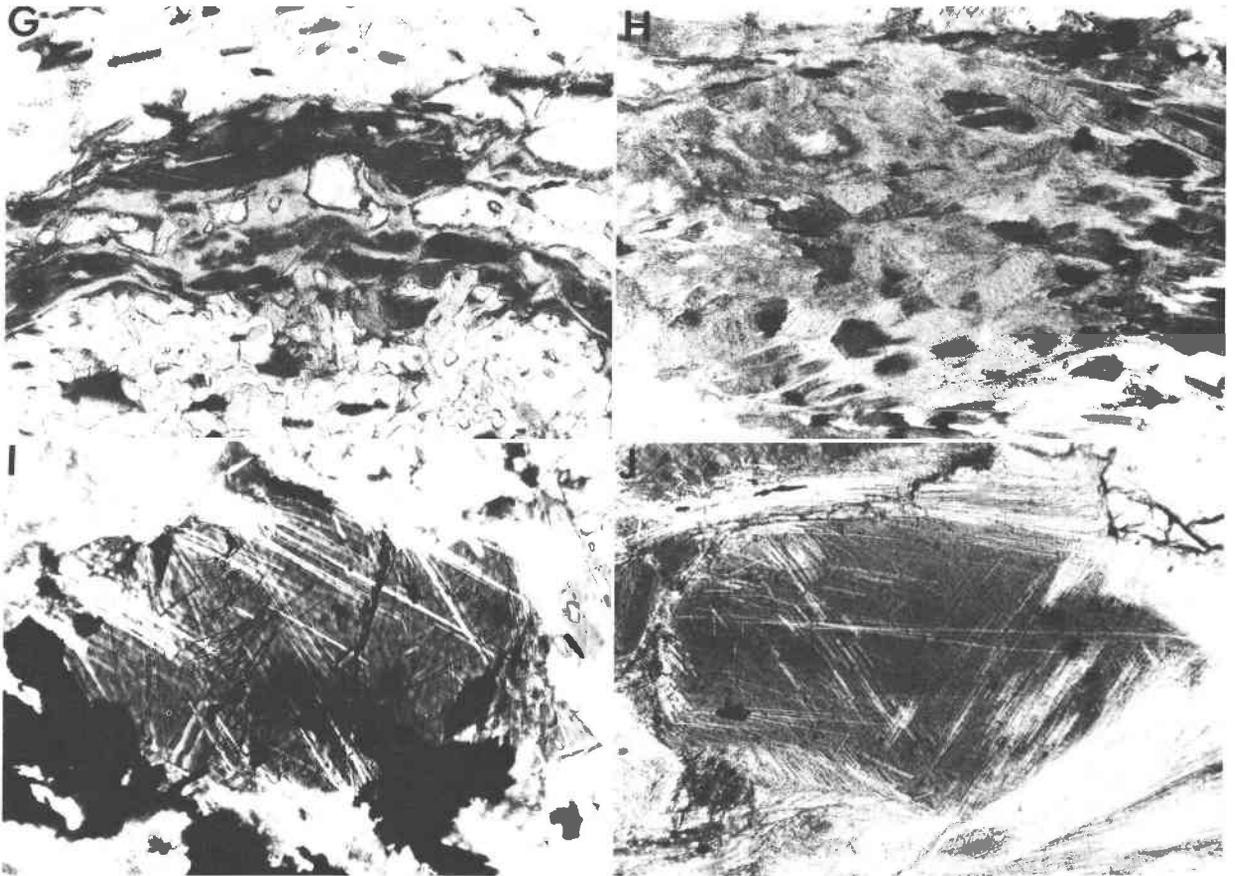
Fig. 2.—*Continued*. (G) Biotite fringed and cut by fibrolite (sample GL-85-10). Width of photo corresponds to 1.3 mm. (H) Remnants of biotite within fibrolite (sample GL-85-8). This represents an advanced stage in the fibrolitization of biotite. Width of photo corresponds to 1.3 mm. (I) Triangular arrangement of fibrolite within the basal plane of biotite (sample ARD-85-1C). Width of photo corresponds to 0.055 mm. (J) Triangular arrangement of fibrolite within the basal plane of biotite. Specimen is a garnet-fibrolite-muscovite-biotite-kyanite-quartz gneiss from Mount Tuckahoe, New York. Width of photo corresponds to 1.3 mm.

quartzofeldspathic dikes and segregations. Thus, growth of the sodic rims may have been influenced by later alkali-rich fluids emanating from the intrusion. The calcic cores thus appear to provide a better representation of the plagioclase equilibrated with the earlier-formed metamorphic assemblage. Accordingly, a pressure of 2.5 ± 0.5 kbar is assumed for the Ardara aureole.

In the kyanite-andalusite zone, kyanite and staurolite occur as inclusions within andalusite porphyroblasts and in the surrounding matrix. Naggar and Atherton (1970), Pitcher and Berger (1972), and Holder (1979) concluded that kyanite and staurolite are aureole minerals that formed before andalusite. This paragenetic sequence is compatible with a prograding aureole passing from the kyanite stability field through to the andalusite stability field. As shown by Kerrick (1968) and Haas and Holdaway (1973), the assemblage kyanite + quartz has a very restricted stability range at the pressure (2.5 kbar) determined by geobarometry. Assuming that the early-formed kyanite crystallized at equilibrium and that the geobarometry is essentially correct, this may suggest that the

fluid phase was somewhat impure, such that in relation to the condition $P_{H_2O} = P_{total}$, the pyrophyllite breakdown curve is shifted to lower temperatures and the kyanite + quartz stability field is thereby enlarged. The coexistence of andalusite + kyanite probably reflects the sluggishness of the kyanite $\rightarrow$ andalusite transformation. Thus, kyanite is considered as a metastable phase during the later andalusite-forming event. Naggar and Atherton (1970) demonstrated that kyanite is restricted to Mg-rich rocks; south of the kyanite zone, higher bulk-rock $Fe/(Fe + Mg)$ ratios precluded kyanite as a phase in the assemblage. Thus, the boundary between the kyanite-andalusite zone and the andalusite zone cannot be interpreted as a prograde isograd reaction.

Figure 4 presents the results of garnet-biotite geothermometry in samples from the Ardara aureole assuming $P = 2.5$ kbar. Some samples were omitted because of the evidence for significant retrogression; i.e., samples ARD-851C and ARD-85-3 contain garnet retrograded to biotite + fibrolite (Fig. 2E), and sample ARD-85-5 contains biotite that has been produced by retrogression of anda-
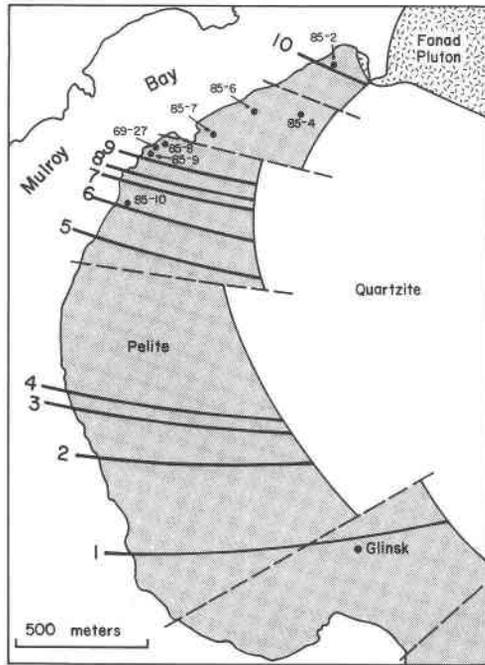
Fig. 3. Sample localities and isograds within a pelitic horizon metamorphosed by the Fanad pluton. The samples are designated with a GL prefix in the text and tables. The isograds are (1) outer limit of new biotite growth, (2) south of this line new biotite is restricted to knots of chlorite, (3) new garnet appears, (4) andalusite appears and chlorite disappears, (5) cordierite appears, (6) fibrolite appears, (7) K-feldspar appears, (8) muscovite disappears, (9) andalusite becomes pleochroic, (10) sillimanite appears. With the exception of isograd (6), which was determined in this study, the isograds are from Pitcher and Berger (1972, Fig. 14-3).

TABLE 5. Ardara aureole samples: Temperatures (°C) from garnet-biotite geothermometry at $P = 2.5$ kbar

Sample no.	T_{FS}*	T_{HS}†	Sample no.	T_{FS}*	T_{HS}†
ARD-69-4	541 ± 19	547	ARD-85-1B	548 ± 19	556
ARD-69-6	492 ± 17	498	ARD-85-1C	647 ± 24	653
ARD-69-7	477 ± 16	484	ARD-85-2A	656 ± 25	661
ARD-69-21	612 ± 23	620	ARD-85-4A	496 ± 17	501
ARD-69-23	510 ± 18	517	ARD-85-5A	527 ± 19	534
ARD-69-25	542 ± 19	554	ARD-85-15	493 ± 17	501
ARD-69-34	621 ± 23	626	ARD-85-16	492 ± 17	499
ARD-69-45	544 ± 19	550	ARD-85-17	484 ± 17	491
ARD-69-63	367 ± 12	387	ARD-85-26A	410 ± 13	435
ARD-69-65B	401 ± 13	425	ARD-85-31A	473 ± 16	481
ARD-85-1A	644 ± 24	648	ARD-85-32A	528 ± 19	535
			ARD-85-33	587 ± 21	592

* T_{FS} = temperatures using the equation of Ferry and Spear (1978). The uncertainties were computed using the standard-error-propagation equation of Hodges and Spear (1982, p. 1126).
† T_{HS} = temperatures using the Ferry and Spear (1978) equation and garnet activity coefficients derived from Equation 9 of Hodges and Spear (1982).

lusite porphyroblasts. Three other samples were rejected on the basis of the presence of quartzofeldspathic dikes or pegmatitic segregations within the thin sections. In these samples, late-stage retrogression may have been fluxed by fluids evolved from the nearby magmatic source.

Figure 4 suggests that the temperature at the sillimanite isograd was between 550 and 600°C. This is in good agreement with Holdaway's (1971) determination of the andalusite = sillimanite equilibrium at 2.5 kbar, thus providing *independent* support for the pressure estimate obtained from the garnet-plagioclase-Al_2SiO_5-quartz equilibrium using core compositions of plagioclase.

The close conformity of the sillimanite isograd to the form of the external intrusive contact supports the interpretation of a uniform thermal profile during metamorphism (as in Fig. 4). Excluding fibrolite, and considering the minor-element contents of andalusite and sillimanite in this aureole, Kerrick and Speer (1987) have concluded that the sillimanite isograd represents a close approximation to the univariant andalusite = sillimanite equilibrium involving pure endmember phases.

Figure 4 suggests that the fibrolite-bearing samples beyond a distance of about 200 m from the intrusive contact formed well below the sillimanite stability field. It is possible that fibrolite in this zone formed at a higher temperature than that recorded by garnet-biotite geothermometry. Accordingly, fibrolite could have formed at the climax of the main thermal event, or by a second thermal pulse, perhaps correlated with the intrusion of the core granodiorite. However, one would expect that the garnet-biotite compositions would have recorded such a higher-temperature history. If contact metamorphism in the Ardara aureole represents a single thermal pulse, as argued by Pitcher and Read (1963), it seems improbable that fibrolitization would have occurred upon progradation without readjustment of the garnet (rim)–biotite compositions to increasing temperature. That garnet-biotite pairs near the sillimanite isograd represent the thermal maximum is supported by the fact that this geothermometer yields reasonable agreement with Holdaway's (1971) andalusite = sillimanite equilibrium at the prevailing pressure. It is therefore suggested that fibrolite formed metastably at temperatures within the andalusite stability field.

These conclusions are based on temperatures derived from the Ferry and Spear (1978) geothermometer. If we instead adopt temperatures from the Hodges and Spear (1982) formulation (Table 5), the thermal profile in Figure 4 would be shallower at distances of 0.5 to 1.0 km from the intrusive contact. However, because the data points for samples near the fibrolite isograd would essentially remain as in Figure 4, there would be little change in the temperatures implied for this isograd. As stated previously, the thermometry for samples 69-63, 69-65B, and 85-26A may be suspect. However, even if these samples were excluded from Figure 4, the remaining data would nevertheless suggest that fibrolite formed at temperatures significantly below the sillimanite stability field.

The thermometry data in Figure 4 are dependent on the assumption that the garnet rim analyses represent equilibrium compositions. For each sample, the garnet analyses given in Table 1 represent the average of several
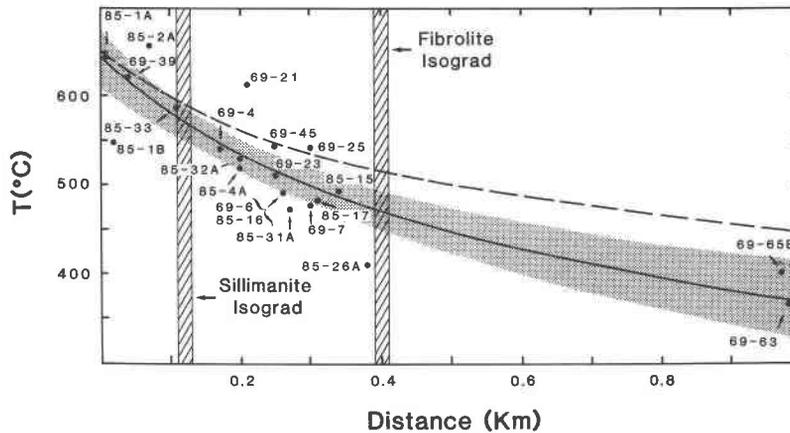
Fig. 4. Plot of temperature as a function of distance from the contact of the Ardara pluton. Temperatures for the data points were derived using the Ferry and Spear (1978) garnet-biotite geothermometer (Table 5). The solid line was obtained by least-squares regression using the equation $T = C_1 + C_2 \ln D$ (where C_1 and C_2 are constants and D = distance). The shaded area encompasses the 95% confidence level about the mean (solid line). The dashed line was calculated assuming heat transfer by conduction only and an intrusion shaped as a vertical cylinder.

point analyses randomly taken within the outer 100 μm of crystals. The random-point procedure was adopted largely as a result of the nature of garnets within andalusite-bearing samples. The presence of abundant, small inclusions within such garnets considerably limited the number of suitable areas for analysis. In these samples, zoning profiles in garnet are unattainable owing to the presence of inclusion-rich cores, or to atoll or skeletal structures. Complete garnet zoning profiles were obtained in three samples (Fig. 5). Garnet-biotite thermometry calculated from the analytical data for sample ARD-85-26A (Fig. 6) yields no consistent temperature variation across this garnet. However, zoning is apparent in the outer portions of garnets in sillimanite-bearing samples ARD-85-1A and ARD-85-1C (Fig. 5). This zoning is reflected in the temperature profiles shown in Figure 6. [Without further analysis, such as that described by Spear and Sel-

verstone (1983), the temperatures derived from garnet core compositions coupled with matrix biotite compositions lack geologic significance.] Thus, for samples ARD-85-1A and ARD-85-1C, garnet compositions determined from averaging random-point analyses in the outer 100 μm provide a source of error in the geothermometry. This factor undoubtedly contributes to the scatter of data points plotted in Figure 4.

It is possible that the *coexistence* of fibrolite with andalusite and/or sillimanite is permitted because of nonstoichiometry. Of particular importance is the coexistence of fibrolite with andalusite, as nonstoichiometry could stabilize this mineral pair to lower metamorphic grades than the sillimanite zone (cf. Fig. 4). To address this question, microprobe analyses were carried out on fibrolite and coexisting andalusite in two specimens from the Ardara aureole (Table 4). [The presence of contami-
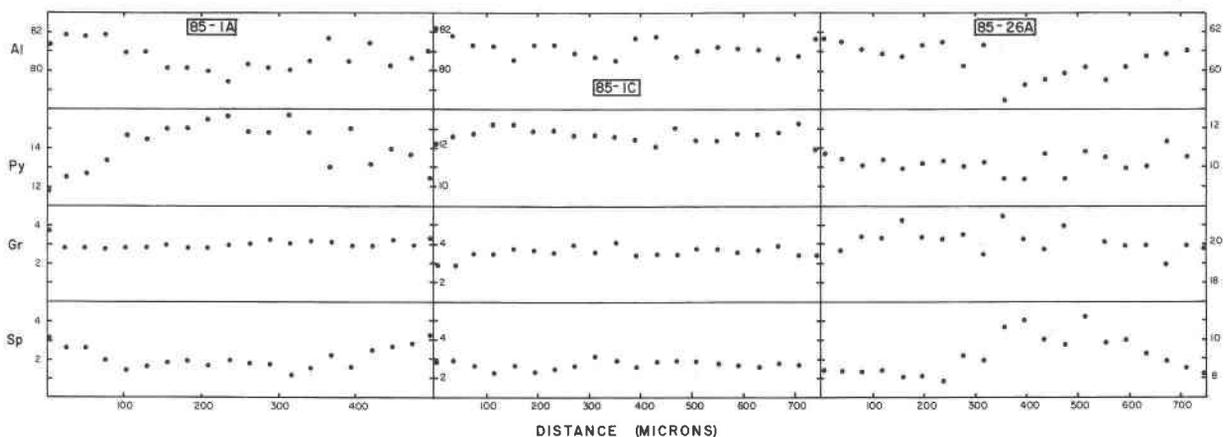
Fig. 5. Mole percentages of components (Al = almandine, Py = pyrope, Gr = grossular, Sp = spessartine) calculated from electron-microprobe traverses across selected garnets from the Ardara aureole.
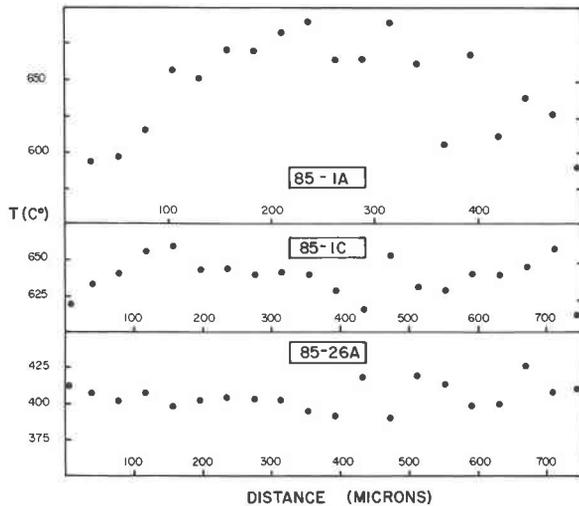
Fig. 6.   Temperatures calculated for electron-microprobe tra-
verses across garnets (see Fig. 5) using the Ferry and Spear (1978)
garnet-biotite geothermometer.

Fig. 7. P-T diagram showing isopleths of selected values of
the equilibrium constant for andalusite = fibrolite equilibrium
($K = X^{\text{fibrolite}}_{VI_{Al}IV_{Al}SiO_5}/X^{\text{andalusite}}_{VI_{Al}IV_{Al}SiO_5}$). The heavy line ($K = 1.0$) corre-
sponds to the equilibrium with stoichiometrically pure phases.

nant phases (especially quartz) in fibrolite precluded anal-
ysis of fibrolite + andalusite pairs in other samples.] As
the andalusite in these samples is colorless, these micro-
probe analyses represent rim compositions (Kerrick and
Speer, 1987). At equilibrium,

$$\Delta G_r = 0 = \Delta G_r^0 + RT \ln K, \qquad (1)$$

where

$$K = a^{\text{Fib}}_{Al_2SiO_5}/a^{\text{And}}_{Al_2SiO_5} = X^{\text{Fib}}_{VI_{Al}IV_{Al}SiO_5}/X^{\text{And}}_{VI_{Al}IV_{Al}SiO_5}.$$

This formulation of the equilibrium constant assumes
ideal mixing in andalusite and fibrolite. For selected K
values, the equilibria in Figure 7 were calculated from
Equation 1 using the VERTEX program of Connolly and
Kerrick (1984, 1987). The standard-state free-energy
change for the reaction (ΔG_r^0) was computed using the
heat-capacity and enthalpy data of Robie and Heming-
way (1984) and the molar volume, thermal expansion,
and compressibility data of Robinson et al. (1982).

As shown in Table 4, samples ARD-85-16 and ARD-
85-17 have respective K values of 0.989 and 0.983. At
2.5 kbar, these equilibrium constants would correspond
to respective temperatures of 585 to 570°C (Fig. 7), i.e.,
20–35 deg below the curve for the pure andalusite = sil-
limanite equilibrium. However, garnet-biotite thermom-
etry for these samples yields temperatures around 490°C.
Providing that the garnet-biotite thermometry yields peak
metamorphic temperatures, it is concluded that nonstoi-
chiometry is insufficient to stabilize fibrolite in these sam-
ples.

Because of the difficulty in quantitatively analyzing
small amounts of light elements with the electron micro-
probe, B was not analyzed in the aluminum silicates in-
vestigated in this study. Grew and Hinthorne (1983) con-

cluded that the relatively low B contents in sillimanite
were insufficient to significantly alter the stability rela-
tions of this phase. Providing that the crystal chemistry
of fibrolite is identical to sillimanite, it is concluded that
B substitution is insufficient to significantly alter the sta-
bility of fibrolite.

Salje's (1986) heat-capacity data suggest that the P-T
stability field of fibrolite is significantly smaller than that
of coarse-grained sillimanite. He has concluded that the
destabilization of fibrolite results from excess energy aris-
ing from lattice defects (stacking faults). Furthermore,
surface free energy would have the effect of destabilizing
fibrolite in relation to coarse-grained sillimanite. Accord-
ingly, within a given contact aureole, fibrolite would be
confined to *higher* metamorphic grades than sillimanite.
However, in the Ardara aureole, fibrolite first appears at
lower metamorphic grades than coarse-grained silliman-
ite. It is therefore concluded that the excess energy of
fibrolite relative to sillimanite is not a significant factor
in the appearance and distribution of fibrolite in this au-
reole.

Within the Fanad aureole, only three samples collected
within the fibrolite zone contain garnet. Thus, this au-
reole yielded considerably less geothermometric data than
samples from the Ardara aureole. In general, tempera-
tures within the andalusite–K-feldspar zone of the Fanad
aureole are in the vicinity of 600°C.

MODEL FOR FIBROLITE FORMATION

The mineral textures in the aureoles investigated in this
study clearly reveal that fibrolite formed from the break-
down of biotite. In several specimens from the Ardara

aureole, this reaction occurred in rocks lacking other Al_2SiO_5 phases; thus, it is concluded that fibrolitization cannot be considered as a polymorphic transformation. Furthermore, local closed-system ionic equilibria linking two aluminum silicate phases, such as suggested by Carmichael (1969) for the kyanite → sillimanite transformation, are precluded for rocks with fibrolite as the sole aluminum silicate.

In the aureoles investigated in this study, evidence has been presented suggesting that the fibrolite formed late in the thermal history of the aureoles. The bulk of the fibrolite appears to have formed from biotite decomposition. The reaction

$$2K(Mg_xFe_{1-x})_3AlSi_3O_{10}(OH)_2 + 14HCl$$
$$= Al_2SiO_5 + 5SiO_2 + 2KCl$$
$$+ 6(Mg_xFe_{1-x})Cl_2 + 9H_2O \quad (1)$$
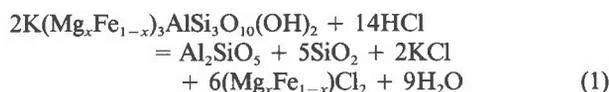
would account for the fibrolitization of biotite. Removal of K, Mg, and Fe as chloride complexes is supported by the efficacy of chlorides as complexing agents. However, petrographic evidence suggests that fibrolite is the dominant phase in the fibrolite-quartz aggregates replacing biotite. Thus, the actual reaction may involve the release of Si as an aqueous complex (e.g., H_4SiO_4). With the exception of one sample (ARD-85-3E), opaque minerals are conspicuously absent in the fibrolite aggregates that have replaced biotite. Accordingly, along with K and Mg, Fe is considered to have been released into the fluid phase. The ultimate fate of the components released into the fluid is unknown. Silica transported as H_4SiO_4 may be deposited nearby as quartz. If late-stage muscovite formed contemporaneously with fibrolite, the muscovite may have provided a local sink for K released from biotite decomposition.

As described by Chinner (1961) for metapelites in the Scottish Highlands, samples from the Donegal aureoles were found to contain fibrolite arranged in a regular trigonal pattern on basal sections of biotite (Fig. 2I). The author has observed this texture in fibrolitized biotite from other localities (Fig. 2J). Flat-stage measurements of the acute angles between the oriented fibrolites typically yield values in the range 58–62°. As suggested by Chinner (1961), this geometric arrangement matches that of the tetrahedral layer of the mica structure (see Liebau, 1980, Fig. 3d). Thus, the nucleation of fibrolite, which contains tetrahedrally coordinated chains parallel to the c axis, was facilitated by the chainlike structure in the tetrahedrally coordinated layers of the host biotite. The formation of the sillimanite (fibrolite) structure from a mica can be envisioned by considering that the tetrahedral chains of the fibrolite were inherited from biotite and that the octahedral sheet of biotite was rearranged upon expulsion of the octahedrally coordinated Mg^{2+} and Fe^{2+}. Loss of the interlayer K^+ resulted in juxtaposition of adjacent tetrahedral chains (as in the sillimanite structure). A key problem is why fibrolite formed rather than andalusite, the polymorph postulated to be stable at the P-T conditions of andalusite-zone rocks. Aside from octahedrally

TABLE 6. Electron-microprobe analyses of fibrolitized vs. non-fibrolitized biotite

	GL-85-8		ARD-85-10*	
	Fibrolitized	Nonfibrolitized	Core	Rim
SiO_2	34.57	34.57	35.13	34.84
Al_2O_3	20.08	20.12	19.29	20.13
TiO_2	3.41	2.54	3.32	2.44
MgO	4.86	5.44	6.70	7.12
FeO	23.67	23.90	22.70	22.23
MnO	0.20	0.15	0.18	0.14
Na_2O	0.09	0.23	0.20	0.14
K_2O	8.85	8.75	8.77	7.85
Cl	—	—	0.03	0.02
Σ	95.73	95.70	96.32	94.91
	Formula basis: 5 oxygens			
Si	5.323	5.333	5.351	5.340
^{IV}Al	2.678	2.667	2.649	2.660
^{VI}Al	0.968	0.990	0.811	0.975
Ti	0.394	0.292	0.380	0.279
Mg	1.115	1.249	1.520	1.624
Fe	3.048	3.082	2.892	2.861
Mn	0.025	0.017	0.022	0.018
Σ	5.550	5.630	5.625	5.757
Ca	—	—	—	—
Na	0.023	0.068	0.058	0.040
K	1.730	1.720	1.703	1.534
Σ	1.753	1.788	1.761	1.574
X_{Phl}	0.202	0.223	0.271	0.283
X_{Ann}	0.552	0.549	0.516	0.499

* Biotite rimmed by fibrolite (see discussion in text).

coordinated Al, the remainder of the Al in the andalusite structure is in fivefold coordination, whereas that in sillimanite is in tetrahedral coordination. The model of fibrolite formation assumes that tetrahedral Al was inherited from the biotite structure. Accordingly, it is postulated that andalusite was precluded because of the additional energy required to rearrange the tetrahedrally coordinated Al of biotite into the AlO_5 hexahedra of andalusite.

Fibrolite is considered to have formed in the waning stages of the thermal event. According to Reaction 1, fibrolitization of biotite would be enhanced by high a_{HCl}. In a recent review, Eugster (1985) has concluded that HCl is evolved from crystallizing granitic magmas. Support for Cl as a major component in volatiles released from the intrusion comes from the fact that Cl is strongly partitioned into the vapor phase (Pichavant, 1983). Hydrolysis reactions such as $2NaCl_{melt} + H_2O = 2HCl_{vapor} + Na_2O_{melt}$ (Eugster, 1985) may be responsible for production of HCl in the magmatic vapor phase. Significant amounts of HCl can also be produced by the crystallization of metal sulfides within the intrusion (Burnham, 1979).

Interpretation of the garnet-biotite geothermometry could be questioned on the basis of the widespread late-stage fibrolitization of biotite. That is, the thermometry would not record maximum temperatures if there were changes in the composition of biotite resulting from the fibrolitization reaction. To test this, electron-microprobe analyses were carried out on samples containing both fi-

brolite-free and fibrolitized biotite. In sample GL-85-8 (from the Fanad aureole), there are no significant differences in the composition of fibrolitized versus fibrolite-free biotite (Table 6). Within a dike cutting sample ARD-85-10 there are relatively large crystals of biotite with peripheral fibrolitization (Fig. 2B). The biotite adjacent to the fibrolite has a slightly different interference color compared to the central portion of the biotite. Electron-microprobe analyses suggest that the biotite adjacent to fibrolite is depleted in Fe and Ti compared to the central portion (Table 6). Nevertheless, the difference in mole fraction of annite and phlogopite between core and rim biotite is approximately 1 mol%. Thus, for thermometric analysis, it is concluded that the fibrolitization reaction has not significantly affected biotite compositions.

Within the sillimanite zone of the Ardara and Fanad aureoles, fibrolite occurs in anastomosing stringers that probably represent fracture fillings. These features were also described by Pitcher and Read (1963) and Pitcher and Berger (1972). The author has observed these textures in metapelites from other contact aureoles. Fibrolite in some samples from the sillimanite zones of the Ardara and Fanad aureoles is confined to grain boundaries of quartz and feldspar (Fig. 2F). However, the bulk of the fibrolite within the andalusite and andalusite-kyanite zones appears to be a replacement product of biotite. Accordingly, the Al for such fibrolite was obtained from the biotite precursor.

Late-stage muscovitization is particularly prominent in the Ardara aureole. Pitcher and Read (1963) and Pitcher and Berger (1972) concluded that fibrolite and muscovite are contemporaneous (or nearly so). On the basis of textures of fibrolite-muscovite intergrowths examined in this study, it is concluded that there is no cogent argument against the contemporaneity of fibrolite and muscovite.

In the Ardara aureole, tourmaline is a prominent accessory in rocks with abundant fibrolite and muscovite. Thus, this study supports Pitcher and Berger's (1972) metasomatic fibrolite-muscovite-tourmaline association. In the Ardara aureole, support for a magmatic source for tourmaline comes from the fact that large tourmaline crystals occur in dikes cutting pelitic schists near the intrusive contact. In fact, Akaad (1956b) noted that a zone of tourmaline ± quartz (varying from 3 to 25 cm in thickness) occurs along the northern and northeastern contacts of the Ardara pluton and that a narrow zone (ca. 2–3 mm) of the adjacent pelite has been replaced by tourmaline. The author examined specimens collected from progressively metamorphosed pelites in the Lettermackaward area, which is considered to be within the aureole of the Thorr pluton. As in the study of Pitcher and Read (1963), there is an increase in the abundance of late-stage fibrolite + muscovite as the intrusive contact is approached. In fact, Pitcher and Berger (1972, p. 307) concluded that "this late-stage encroachment of a metasomatic zone seems to be a general feature of the Donegal aureoles." Thus, the conclusion is arrived at that, in addition to HCl, the fluids evolved from the cooling intrusion re-

leased B. Such metasomatic fluids may also have been active in some regionally metamorphosed rocks. For example, the presence of B-enriched fluids in the late-stage fibrolitization of granulite-facies rocks was documented in the study of Ahmad and Wilson (1981).

Experimental data show that, for systems containing Cl and B, the magmatic vapor phase should be enriched in K and Na. Thus, it is probable that the fluid carried Na in addition to K. In the Ardara aureole, it is possible that the Na-enriched rims on plagioclase reflect the sink for the Na of the metasomatic fluid.

There is no cogent evidence bearing on the relative timing of the fibrolitization of biotite versus the development of the metasomatic fibrolite-muscovite-tourmaline assemblage. If we assume that these processes were contemporaneous, fibrolitization by Reaction 1 would be enhanced by low a_{KCl} in the metasomatic fluid. Providing that the development of the sodic rims on plagioclase was contemporaneous with a single fibrolite-forming event, it is possible that the metasomatic fluid had a relatively high a_{NaCl}/a_{KCl} ratio. This is in concert with the experimental data of Burnham (1967), which showed that fluids in equilibrium with granitic material at 650°C and 6 kbar have molar NaCl/KCl ratios in the range 1.8–1.9. Development of muscovite would have been favored by KCl released from the fibrolitization of biotite (Reaction 1).

Aside from the areas investigated in this study, there are other contact aureoles where fibrolite first appears at lower grade than coarse sillimanite (Woodland, 1963; Loomis, 1972; Blümel and Schreyer, 1976; Woodsworth, 1979; Speer, 1982). In the aureoles studied by Loomis (1972), Woodsworth (1979), and Speer (1982), the biotite-fibrolite association is common. Thus, the mechanism proposed in this study may be a common phenomenon in contact-metamorphosed metapelites.

Late-stage fibrolitization has also been postulated in several studies of regionally metamorphosed pelites (Chinner, 1966; Chakraborty and Sen, 1967; Ashworth, 1975). In a regionally metamorphosed sequence in the Mount Mossilauke area of New Hampshire, Rumble (1973) showed that fibrolite is widely distributed in rocks containing sillimanite and/or andalusite. The fibrolite is typically associated with biotite or muscovite. In the Plymouth quadrangle, Rumble (1973, Fig. 1) showed numerous localities where fibrolite occurs without coexisting andalusite or sillimanite. Accordingly, this area may have experienced late-stage fibrolitization. The numerous granitic intrusions in this area could have provided a source for acidic volatiles needed for the fibrolitization. Within the Ticino thermal high of the Lepontine Alps of Switzerland, representing a Barrovian regional metamorphic regime, the author has found an extensive zone (12 km in width) of fibrolite within the upper kyanite zone. Much of the fibrolite in this area formed as a replacement of biotite. Bühl (1981) concluded that fibrolite formed during retrograde metamorphism in sillimanite-zone gneisses of this area. Within the Lepontine Alps there occur spectacular Al_2SiO_5-quartz-feldspar segregations

containing abundant tourmaline; these segregations are considered to have formed in the waning stages of the thermal event (Kerrick et al., 1985). Thus, as in the Donegal aureoles, B is considered as a constituent of the late-stage fluids.

Ferry's (1983) study suggests that acid metasomatism may be important in regional metamorphism. Thus, the mechanism of fibrolitization of biotite by influx of HCl-bearing fluids could well account for fibrolitized biotite in many regionally metamorphosed pelites. It must be emphasized, however, that fibrolite is not a late-stage mineral in all regionally metamorphosed pelites. In the Truchas Peak region of New Mexico (Grambling, 1981) and in the Mica Creek region of British Columbia (E. D. Ghent, pers. comm.), fibrolite and coarse sillimanite appear together at the first sillimanite isograd in these regionally metamorphosed terranes.

Note added in proof. Subsequent to final checking of the page proofs of this paper, I became aware of J.A.T. Smellie's (1974) paper on the genesis of atoll garnets in metapelites of the Ardara aureole. He concluded that most garnets display varying degrees of replacement by biotite + plagioclase + quartz + opaques. In some samples, this replacement reaction progressed inward from the exterior portions of garnet crystals, whereas in others, the replacement reaction began in the interiors of garnet crystals. Smellie concluded that garnet atoll structures formed in the advanced stages of replacement. From analysis of garnet zoning profiles, it was concluded that the replacement reaction yielded reversed zoning characterized by depletion in Ca and Mg in the peripheral regions of resorbed garnets. The garnet profiles shown in Figure 5 of the present contribution were obtained on relatively large, rounded garnet crystals. According to Smellie's interpretation, such garnets would be least affected by the replacement reaction. The garnet zoning profiles of samples 85-1A and 85-26A (Fig. 5) were obtained from crystals lacking textural evidence for replacement. However, the garnet in sample 85-1C contains fibrolite in the core, thereby implying that replacement occurred in the interior. Following Smellie's analysis, the lack of detectable Ca depletion in the rims of the garnets plotted in Figure 5, coupled with similar compositions of the rims on each garnet crystal (Fig. 5), suggests that the peripheral regions of garnets in Figure 5 were not affected by the replacement reaction. Nevertheless, Smellie suggested that reverse zoning is common in the outer 25 μm of garnet crystals of metapelites in the Ardara aureole. Accordingly, his data support the conclusion (p. 249) that compositional zoning provides a source of error for the garnet analyses of Table 1, which were obtained by averaging random points within in the outer 100 μm of crystals.

Garnet atoll structure is present in samples 69-7, 85-1C, 85-17, and 85-32A. Garnets in samples 69-34, 69-45, 69-63, 85-15, and 85-33 have "dusty" centers that *may* reflect incipient replacement of the central portions. Garnets analyzed in other samples (Table 1) lack textural evidence of replacement. Inspection of the geothermometric data as a function of distance from the intrusive contact (Fig. 4) reveals no consistent differences between the above three textural groups of garnet. Accordingly, the garnet replacement reaction does not appear to complicate the interpretation of the thermal profile of the aureole as derived from garnet-biotite thermometry (Fig. 4).

References

Ahmad, R., and Wilson, C.J.L. (1981) Uranium and boron distributions related to metamorphic microstructure—Evidence for metamorphic fluid activity. Contributions to Mineralogy and Petrology, 76, 24–32.

Akaad, M.K. (1956a) The Ardara granitic diapir of Co. Donegal, Ireland. Geological Society of London Quarterly Journal, 112, 263–288.

——— (1956b) The northern aureole of the Ardara pluton of Co. Donegal. Geological Magazine, 93, 377–392.

Albee, A.L., and Ray, L. (1970) Correction factors for electron probe microanalysis of silicates, oxides, carbonates, phosphates and sulfates. Analytical Chemistry, 42, 1408–1414.

Ashworth, J.R. (1975) The sillimanite zones of the Huntly-Portsoy area in the north-east Dalradian, Scotland. Geological Magazine, 112, 113–224.

Bell, P.M., and Nord, G. (1974) Microscopic and electron diffraction study of fibrolitic sillimanite. Carnegie Institution of Washington Year Book 73, 444–448.

Blümel, P., and Schreyer, W. (1976) Progressive regional low-pressure metamorphism in Moldanubian metapelites of northern Bavarian Forest, Germany. Krystalinikum, 12, 7–30.

Bühl, H. (1981) Zur sillimanitbildung in den gneisen der zone von Bellinzona. Schweizerische Mineralogische und Petrographische Mitteilungen, 61, 275–295.

Burnham, C.W. (1967) Hydrothermal fluids at the magmatic stage. In H.L. Barnes, Ed. Geochemistry of hydrothermal ore deposits, p. 34–76. Holt, Rinehart, & Winston, New York.

——— (1979) Magmas and hydrothermal fluids. In H.L. Barnes, Ed. Geochemistry of hydrothermal ore deposits, p. 71–136. Wiley, New York.

Carmichael, D.M. (1969) On the mechanism of prograde metamorphic reactions in quartz-bearing pelitic rocks. Contributions to Mineralogy and Petrology, 20, 244–267.

Chakraborty, K.R., and Sen, S.K. (1967) Regional metamorphism of pelitic rocks around Kandra, Singhbhum, Bihar. Contributions to Mineralogy and Petrology, 16, 210–232.

Chinner, G.A. (1961) The origin of sillimanite in Glen Clova, Angus. Journal of Petrology, 2, 312–323.

——— (1966) The distribution of pressure and temperature during Dalradian metamorphism. Geological Society of London Quarterly Journal, 122, 159–186.

Connolly, J.A.D., and Kerrick, D.M. (1984) VERTEX: A computer algorithm for the calculation of stable phase assemblages and Schreinemakers-type phase diagrams (abs.). EOS, 65, 287.

——— (1987) An algorithm and computer program for calculating composition phase diagrams. CALPHAD, 11, 1–61.

Edmunds, W.M. (1969) A chemical and mineralogical study of hornfelses in County Donegal. Ph.D. thesis, University of Liverpool.

Edmunds, W.M., and Atherton, M.P. (1971) Polymetamorphic evolution of garnet in the Fanad aureole, Donegal, Eire. Lithos, 4, 147–161.

Eugster, H.P. (1985) Granites and hydrothermal ore deposits: A geochemical framework. Mineralogical Magazine, 49, 7–23.

Ferry, J.M. (1983) Regional metamorphism of the Vassalboro Formation, south-central Maine, USA: A case study of the role of fluid in metamorphic petrogenesis. Geological Society of London Journal, 140, 551–576.

Ferry, J.M., and Spear, F.S. (1978) Experimental calibration of the partitioning of Fe and Mg between biotite and garnet. Contributions to Mineralogy and Petrology, 66, 113–117.

Finger, L.W., and Prince, E. (1972) Neutron diffraction studies: Andalusite and sillimanite. Carnegie Institution of Washington Year Book 71, 496–500.

Ghent, E.D. (1976) Plagioclase-garnet-Al₂SiO₅-quartz: A potential geobarometer-geothermometer. American Mineralogist, 61, 710–714.

Ghent, E.D., Robbins, D.B., and Stout, M.Z. (1979) Geothermometry, geobarometry, and fluid compositions of metamorphosed calc-silicates and pelites, Mica Creek, British Columbia. American Mineralogist, 64, 874–885.

Grambling, J.A. (1981) Kyanite, andalusite, sillimanite, and related assemblages in the Truchas Peaks region, New Mexico. American Mineralogist, 66, 702–722.

Grew, E.S., and Hinthorne, J.R. (1983) Boron in sillimanite. Science, 221, 547–549.

Haas, H., and Holdaway, M.J. (1973) Equilibria in the system Al₂O₃-SiO₂-H₂O involving the stability limits of pyrophyllite. American Journal of Science, 273, 449–464.

Halliday, A.N., Aftalion, M., and Leake, B.E. (1980) A revised age for the Donegal granites. Nature, 284, 736–737.

Hodges, K.V., and Spear, F.S. (1982) Geothermometry, geobarometry and the Al₂SiO₅ triple point at Mt. Moosilauke, New Hampshire. American Mineralogist, 67, 1118–1134.

Holdaway, M.J. (1971) Stability of andalusite and the aluminum silicate phase diagram. American Journal of Science, 271, 97–131.

Holder, M.T. (1979) An emplacement mechanism for post-tectonic granites and its implication for their geochemical features. In M.P. Atherton and J. Tarney, Eds. Origin of granite batholiths: Geochemical evidence, p. 116–128. Shiva.

Kerrick, D.M. (1968) Experiments on the upper stability limit of pyrophyllite at 1.8 kb and 3.9 kb water pressure. American Journal of Science, 266, 204–214.

——— (1986) Dislocation strain energy in the Al₂SiO₅ polymorphs. Physics and Chemistry of Minerals, 13, 221–226.

Kerrick, D.M., and Heninger, S.G. (1984) The andalusite-sillimanite equilibrium revisited. Geological Society of America Abstracts with Programs, 16, 558.

Kerrick, D.M., and Speer, J.A. (1987) The role of minor element solid solution on the andalusite-sillimanite equilibrium in metapelites and peraluminous granitoids. American Journal of Science, in press.

Kerrick, D.M., Mullis, J., and Klein, H. (1985) Al₂SiO₅-bearing segregations in the Lepontine Alps, Switzerland: Aluminum mobility in metapelites. Geological Society of America Abstracts with Programs, 17, 627.

Liebau, F. (1980) Classification of silicates. Mineralogical Society of America Reviews in Mineralogy, 5, 1–24.

Loomis, T.P. (1972) Contact metamorphism of pelitic rock by the Ronda ultramafic intrusion, southern Spain. Geological Society of America Bulletin, 83, 2449–2474.

Naggar, M.H., and Atherton, M.P. (1970) The composition and metamorphic history of some aluminum silicate-bearing rocks from the aureoles of the Donegal granites. Journal of Petrology, 11, 549–589.

Navrotsky, A., Newton, R.C., and Kleppa, O.J. (1973) Sillimanite-disordering enthalpy by calorimetry. Geochimica et Cosmochimica Acta, 37, 2497–2508.

Newton, R.C., Charlu, T.V., and Kleppa, O.J. (1977) Thermochemistry of the high pressure garnets and clinopyroxenes in the system CaO-MgO-Al₂O₃. Geochimica et Cosmochimica Acta, 41, 369–377.

Okrusch, M., and Evans, B.W. (1970) Minor element relationships in coexisting andalusite and sillimanite. Lithos, 3, 261–268.

Peterson, R.C., and McMullan, R.K. (1986) Neutron diffraction studies of sillimanite. American Mineralogist, 71, 742–745.

Pichavant, M. (1983) Melt-fluid interaction deduced from studies of silicate-B₂O₃-H₂O systems at 1 kbar. Bulletin de Minéralogie, 106, 201–211.

Pitcher, W.S. (1965) The aluminum silicate polymorphs. In W.S. Pitcher and G.W. Flinn, Eds. Controls of metamorphism, p. 327–341. Wiley, New York.

Pitcher, W.S., and Berger, A.R. (1972) The geology of Donegal: A study of granite emplacement and unroofing, 435 p. Wiley, New York.

Pitcher, W.S., and Read, H.H. (1963) Contact metamorphism in relation to manner of emplacement of the granites of Donegal, Ireland. Journal of Geology, 71, 261–296.

Powell, D., and Phillips, W.E.A. (1985) Time and deformation in the Caledonide orogen of Britain and Ireland. In P.L. Harris, Ed. The nature and timing of orogenic activities in the Caledonian rocks of the British Isles. Geological Society of London Memoir 9, 17–39.

Robie, R.A., and Hemingway, B.S. (1984) Entropies of kyanite, andalusite, and sillimanite: Additional constraints on the pressure and temperature of the Al₂SiO₅ triple point. American Mineralogist, 69, 298–306.

Robinson, G.R., Jr., Haas, J.L., Jr., Schafer, C.M., and Haselton, H.T., Jr. (1982) Thermodynamic and thermophysical properties of selected phases in the MgO-SiO₂-H₂O-CO₂, CaO-Al₂O₃-SiO₂-H₂O-CO₂, and Fe-FeO-Fe₂O₃-SiO₂ chemical systems, with special emphasis on the properties of basalts and their mineral components. U.S. Geological Survey Open-File Report 83–79, 429 p.

Rumble, D., III. (1973) Andalusite, kyanite and sillimanite from the Mount Moosilauke region, New Hampshire. Geological Society of America Bulletin, 84, 2423–2430.

Salje, E. (1986) Heat capacities and entropies of andalusite and sillimanite: The influence of fibrotitization on the phase diagram of the Al₂SiO₅ polymorphs. American Mineralogist, 71, 1366–1371.

Sanderson, D.J., and Meneilly, A.W. (1981) Analysis of three-dimensional strain modified uniform distributions: Andalusite fabrics from a granite aureole. Journal of Structural Geology, 3, 109–116.

Smellie, J.A.T. (1974) Formation of atoll garnets from the aureole of the Ardara pluton, Co. Donegal, Ireland. Mineralogical Magazine, 39, 878–888.

Spear, F. S., and Selverstone, J. (1983) Quantitative P-T paths from zoned minerals: Theory and tectonic applications. Contributions to Mineralogy and Petrology, 83, 348–357.

Speer, J.A. (1982) Metamorphism of the pelitic rocks of the Snyder Group in the contact aureole of the Kiglapait layered intrusion, Labrador: Effects of buffering partial pressures of water. Canadian Journal of Earth Sciences, 19, 1888–1909.

Vernon, R.H. (1979) Formation of late sillimanite by hydrogen metasomatism (base-leaching) in some high-grade gneisses. Lithos, 12, 143–152.

Woodland, B.G. (1963) A petrographic study of thermally metamorphosed pelitic rocks in the Burke Area, northeastern Vermont. American Journal of Science, 261, 354–375.

Woodsworth, G.J. (1979) Metamorphism, deformation, and plutonism in the Mount Raleigh pendant, Coast Mountains, British Columbia. Canadian Geological Survey Bulletin, 295, 58 p.

Zen, E-An. (1969) The stability relations of the polymorphs of aluminum silicate: A survey and some comments. American Journal of Science, 276, 297–309.